Studies of banded spherulitic growth in an ethylene-carbonate–polyacrylonitrile mixture

Laurent Talon
45 rue d'Ulm
75005 Paris
FRANCE
Supervisor: John Bechhoefer
Simon Fraser University, Burnaby, B.C, CANADA

August 1, 2000

Contents

Abstract

I studied the solidification of an ethylene-carbonate–polyacrylonitrile at high undercooling. When the undercooling is high enough, the solidification growth shows a periodic morphology identified as banded spherulites. Although this growth mode is not well-understood, it can been seen with in many different materials. I investigated this regime in an ethylene-carbonate–polyacrylonitrile mixture. I tried determine whether the patterns seen in that material have properties similar to those seen in other systems. I also measured the periodicity as a function of different parameters such as the undercooling, sample thickness, and polymer concentration.

———————————————————

Au cours de ce stage, j'ai étudié la solidification d'un mélange d'éthylène-carbonate–polyacrylonitrile pour des températures de surfusion élevées. Lorsque la surfusion est suffisament élevée, la morphologie de solidification devient périodique, celle-ci est appelée sphérulites à bandes. Bien que ce regime de solidification a été observé pour de nombreux materiaux differents, son origine n'a jamais été expliquée. J'ai étudié ce regime dans le cas particulier du m'élange éthylène-carbonate–polyacrylonitrile. J'ai éssayé de vérifier si la périodicité observée avait les mêmes propriétées que pour les autres types de materiaux pour m'assurer que le phénomène était bien le même. J'ai aussi tenté d'évaluer l'influence de divers paramètres comme la température de surfusion, l'épaiseurs des échantillons ou la concentration en polymère.

Chapter 1

Introduction

The free-growth solidification of a fluid is a very old problem. The physics involved in the solidification of low-viscosity fluids is relatively well understood, but not so for high-viscosity fluid.

In thermodynamic equilibrium, phase transitions appear when the Gibbs free energy of one state is higher than the free energy of another potential state of the system. Thermodynamics tells us that a phase transition between liquid and solid should occur at a fixed temperature T_0. However, a liquid state is usually seen at temperature below this threshold. This state is "metastable" because the free energy shows a local minimum, even though this state is not the most stable among all the possible states. The temperature difference between the metastable liquid and T_0 is called "undercooling" and represented $\Delta T = T_0 - T$. The solidification growth depends strongly on the value of ΔT. Many studies have been made to investigate the shape of the solidification growth for a given system and particular undercooling. Currently, it is still impossible to predict which mode will been seen for a particular ΔT. although, some theories have claimed to model different regimes.

At low undercooling, a typical regime is called dendritic and is shown in Fig. 1.1(a). As the undercooling increase, one usually sees a spherulitic regime characterized by the radial symmetry. For more higher undercooling, a banded spherulitic growth appears, characterized by his radial symmetry as the spherulitic groth but with a concentric-circle periodicity (Fig. 1.1(b)).

This last regime appears in many kinds of materials, including polymers, organic liquids, liquid crystals. Although this mode has been studied for over a century, nobody has been able to give a coherent theory for the phenomenon—or even tell what are the physical laws that are involved in such a system. For example, in pure polymer as in liquid crystals, the band spacing λ is always of the order of few microns. By contrast, a recently studied system, maleic ahydride and polyacrylonitrile (MA-PA), shaws bands with $\lambda \approx 1$ cm. At present, there is no theory that predicts the scale of λ in any of these cases.

Nonetheless, previous studies have suggested that a twist of the crystal might be responsible for these bands. A model due to Owen [2], who was continuing the study of Keith and Padden

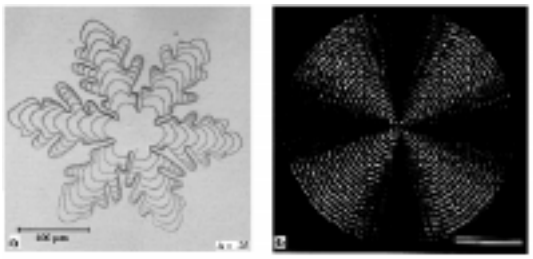

Figure 1.1: Different kind of regime: (a) Dendrtitic regime. (b) Banded-spherulitic regime.

[3], predicts that the band spacing λ should obey the law $\lambda \propto \Delta T^{-1.5}$. Recently, in a study of the maleic-anhydride–polyacrylonitrile mixture, M. Degen, N. Costanzino, and J. Bechhoefer [1], observed a law close to that theory. They noted that although the observed powerlaw diverges at $\Delta T = \Delta T^* \approx 0$, one cannot see bands for $\Delta T < 8.3^o C = \Delta T_\infty$. To reconcile those two observations, they examined another property of the banded spherulites, which is the presence of a "core region." The core region is defined by the area between the spot of the nucleation and the first dark band. In maleic anhydride, it appears that the size of this region diverges at $\Delta T = \Delta T_\infty$ (Fig. 1.2), explaining why bands cannot be seen seen for $\Delta T < \Delta T_\infty$.

My goal was to make a similar study using another material (ethylene-carbonate (EC) and polyacrylonitrile (PA)), which was already started by M. Degen and M. Case. The advantage of this kind of mixture is that the bands are large ($\lambda \approx$ 1mm as shown in Fig. 1.3), and that the chemical properties are more convenient (the polymer was not soluble enough in the case of maleic anhydride, causing phase separation in the liquid) I will show that if common features of the mode can still be seen, the laws observed slightly different from those obtained in the former study. In particular, the band spacing does not diverge at $\Delta T^* \approx 0^o C$ but at $\Delta T^* \approx 5^o C$. I also investigated the dependence of band spacing on the viscosity of the mixture.

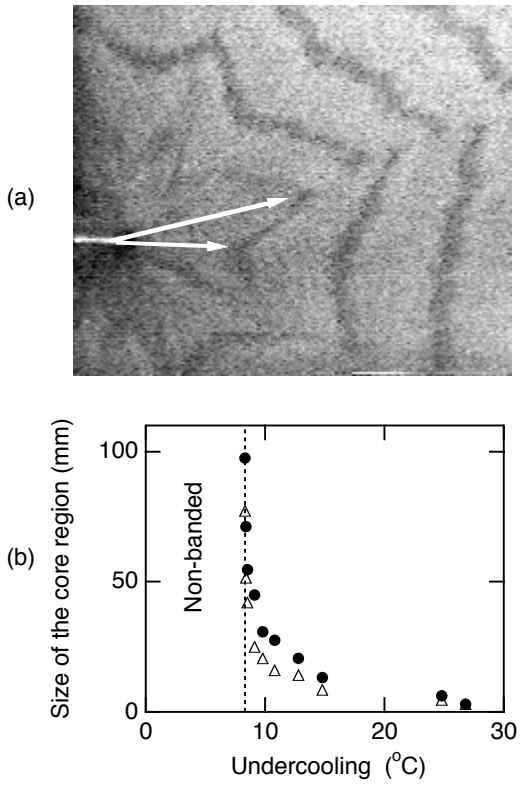

Figure 1.2: (a) Photograph showing the core region and first few bands of a banded spherulite grown at $\Delta T = 24.9\,^{\circ}\mathrm{C}$, in a 2% mixture of polyacrylonitrile in maleic anhydride. The probe used to induce nucleation is visible on the left side of the image and two lines indicate the relevant distances to the first band. (b) Size of the core region vs. undercooling. (•) denotes the maximum size of the core region and (△) the minimum. (Data taken by M. Degen and M. Case)

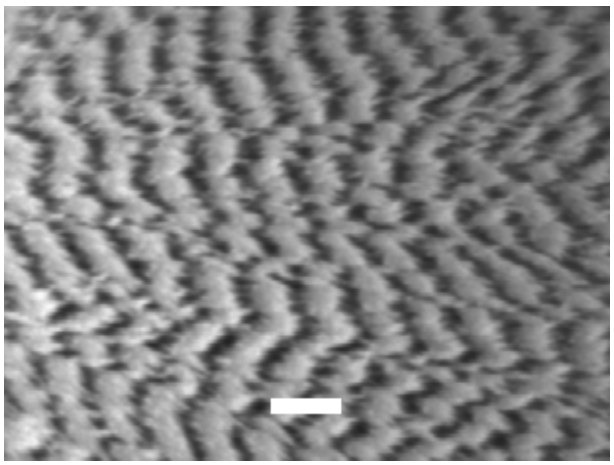

Figure 1.3: Banded spherulitic growth in a 6.2% mixture of polyacrylonitrile in ethylene carbonate. $T = 28.86^{o}C$ (undercooling $\Delta T = 6.34^{o}C$). Scale bar is 1 mm.

Chapter 2

Theoretical background

In this chapter, I will give some solidification theorie, in order to understand better how a solidification starts, how it grows and how it can leads to a spheruilitic patterns.

In section 2.1, I will explain why metastable state are observed and how the solidification can be started. In section 2.2, I will give an example of one regime of solidification in order to give an idea of the physical effects that are involved in our system. In section 2.3 I will present some models proposed to explain the banded spherulites growth. A model of "elastic twist", in particular, has been proposed by Keith and Padden, and later developed by Owen.

2.1 Nucleation

If the temperature of the system is below the melting point, the liquid state is not stable. However, the system does not necessarily change its state, as there is an energy barrier between these two state. The barrier results from the fact that an interface has to be created to form a solid phase. Creating an interface will increase the free energy. Creating a spherical solid germ will modify the free energy by two different effects: an increase of the Gibbs free energy due to the new interface and a decrease due to the transformation from liquid into solid:

$$\Delta G = \frac{4}{3}\pi R^3 \Delta\mu + 4\pi R^2 \gamma, \tag{2.1}$$

where $\Delta\mu$ is the change of chemical potential per unit of volume (which is negative), γ is the surface energy per unit of area and R the radius of the germ. To initiate the crystallization, one needs a germ whose radius is greater than a critical value R^* defined by

$$\frac{\partial G}{\partial R} = 4\pi R^{*\,2}\Delta\mu + 8\pi R^*\gamma = 0. \tag{2.2}$$

Leading to

$$R^* = -\frac{2\gamma}{\Delta\mu}. \tag{2.3}$$

Of course, $\Delta\mu$ depends on the undercooling. Denoting by $\mu^s(T)$ and $\mu^l(T)$ the chemical potentials of the solid and liquid respectively, and T_0 is the solid-liquid coexistence temperature, we can approximate $\Delta\mu$ by

$$\begin{aligned} \Delta\mu = \mu^s(T) - \mu^l(T) &= [\mu^s(T_0) - (T - T_0)s_s] - [\mu^l(T_0) - (T - T_0)s_l], \\ &\approx L\frac{\Delta T}{T_0}, \end{aligned} \tag{2.4}$$

using

$$\begin{cases} L = T_0\Delta S, \\ \mu^l(T_0) = \mu^s(T_0), \end{cases} \tag{2.5}$$

Finally,

$$R^* = \frac{2\gamma T_0}{L\Delta T} = 2d_0\frac{T_0}{\Delta T}, \tag{2.6}$$

where $d_0 = \frac{\gamma}{L}$ is known as the capillarity length. It is typically a few angstroms. Thus, the critical radius decreases when the undercooling increases. As the critical radius decreases, it is more and more likely that thermal fluctuations form a germ whose radius exceeds the critical one. This explains why there is a relatively well-defined critical undercooling, above which the probability to form a germ spontaneously is so great that we cannot see the metastable state for a long enough time to do our experiment. Experimentally, the critical undercooling was about 20^oC in EC-PA, but this threshold depends sensitively on the amount of impurities in the mixture. In particular, we observed critical undercooling ranging from 20^oC to 30^oC depending on how well we did cleaned the glass and the copper substrate that bounded each sample. The fact that there is a critical radius explains the existence of a front solidification instead of many crystals creating throughout the system at the same time.

2.2 Solidification regimes

Now we have an idea of how the solidification starts, the next step in the study is to understand how the germs grow. For this, we need to know the physical effects that determine the shape of the crystals. In other terms, we need to know what kinds of phenomena might determine the velocity of crystal growth as a function of the external parameters. Possible effects that might determine the velocity of the crystallization

- Faceting of the crystal (if the crystal has facets). Since some facets may grow faster than other. This effect can be seen in snowflake, for example.
- Thermal transfer. Since the solidification of a liquid releases latent heat, the temperature of the liquid tends to increase around the interface. One can easily understand that the front velocity can be determine by the heat transport that can be by diffusion, convection or radiation. This effect is dominant in the snow-flakes growth and in the dentritic growth which I will discussed later

- Impurity diffusion. If there are some impurities in the liquid, the concentration of those impurities can be different in the liquid than in the solid. During the solidification, some impurities will be release or disappear that will induce a gradient of concentration. The front growth might therefore depends on the diffusion of those impurities.

- Hydrodynamic flow in the fluid. Because the densities of the solid and the liquid are different (in most of cases the solid is more dense), some materials has to flow to the front. This liquid-flow might limit the solidification growth.

- Attachement kinetics. In the solid, the molecules have an ordered position whereas in the liquid they are disorganized. Every molecule have to be in the particular position to go from the liquid state to the solid state. The solidification velocity can be limited by how fast the molecules go to the particular orientation needed in the ordered phase.

I will discuss more precisely the diffusion-limited regime and how it leads to dentritic growth, as the ideas are relevant to Tiller [4] for the transition between the dendritic regime and the spherulitic regime.

2.2.1 Heat-diffusion equations

The diffusion equation determine the temperature field $T(x, y, z)$ in the system. The field satisfies the following equation:

$$\frac{\partial T}{\partial t} = D_h \nabla^2 T, \tag{2.7}$$

where D_h is the thermal diffusion constant.

The following boundary conditions are used:

$$\begin{cases} T(z \to +\infty) = T_\infty, \\ T_{int} = T_0(1 - d_0\kappa), \\ -D_{h\,l}\rho_l(\vec{\nabla}T)_l + D_{h\,s}\rho_s(\vec{\nabla}T)_s = L(\vec{v}\cdot\hat{n})\hat{n} \end{cases} \tag{2.8}$$

The second boundary condition is the Gibbs–Thompson equation, which gives the temperature of liquid-solid coexistence for a curved interface in terms of the flat interface. Here κ is the mean curvature of the liquid-solid interface. The third equation gives the discontinuity of the temperature-gradient at the interface due to the latent heat, where $\rho_{s/l}$ is the density of the solid and liquid, and $\hat{n}$ is a vector normal to the interface.

The impurities equation are analogous to those equations. One has to substitute the diffusion constants and to replace the latent heat with the difference of the impurity-concentration in the solid and in the liquid. In our case, the impurity-diffusion does not seem to be significant.

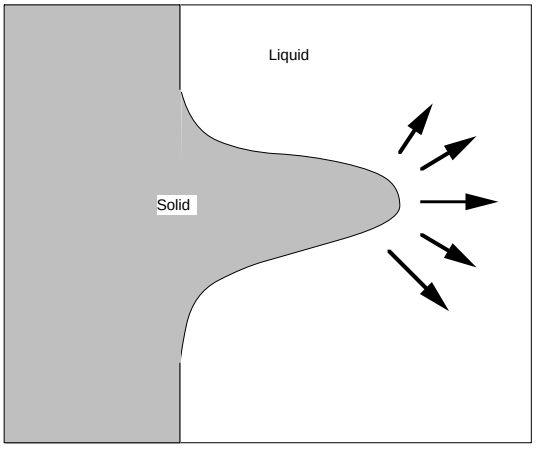

Figure 2.1: Mullins-Sekerka instability

Mullins and Sekerka [5] showed with those equations that a planar front growing are typically unstable to small shape perturbations in the diffusion-limited regime. The gist of their argument is the following: solidification velocity of solidification depends on $\Delta\mu = \mu^s(T) - \mu^l(T)$, which increases with undercooling. During solidification, the temperature of the front will increase, reducing the velocity. A small protusion will destabilize the planar front, as shown in Fig. 2.1, by creating a larger temperature gradient around the tip, which will cool more quickly and thus lead to faster growth of the front.

This kind of phenomena will lead to the dendritic mode. This regime was seen in our mixture for small undercooling. Tiller [4] proposed that the core region is dendritic and that there is a dendrite-to-spherulite transition at a finite distance from the nucleation point.

2.2.2 Spherulites

A feature common to all spherulitic growth is that the resulting structure has an approximate radial symmetry, whereas the dendritic patterns shows crystallographic side-branching. Tiller [4] has proposed that the observed radial splay of crystallites is due to a viscous flow induced by the density difference between liquid and solid. This density difference forces the fluid to flow through the narrow channels between crystallites. This flow generates viscous stresses, which can bend or even break the dentrites

2.3 Model of banded spherulites regime

It has been observed that the bands seen in this regime are associated with a rotation of the optical axis. This optical rotation has two possible causes. The first is that there is a statistical rotation

of the crystals. The other is that each crystallites is twisting. An explanation of the rotation of the crystallites was given by Faivre [7], corresponding to an accumulation of defects. Twist can be explained by the presence of stress on the crystallites. This stress might come from a surface-tension difference or from an hydrodynamical flow. I will present in this section the model given first by Keith and Padden, assuming that the twist is elastic and due to surface-tension difference [6]. One can notice that if the stress was due to an hydronamical flow, the effect of this one should depends on the viscosity and on the density difference between the solid and the liquid.

Consider the work W required to bend elastically a plate of thickness t and elastic modulus α to a radius of curvature R. Then we have, according to elastic theory [8],

$$W \propto \frac{\alpha t^3}{R^2}. \tag{2.9}$$

By envisioning that two such bent plates may be connected end to tail, it is easy to see that the periodicity should be of order

$$\lambda \propto R. \tag{2.10}$$

From Eqs. 2.9 and 2.10, we see that the periodicity is

$$\lambda \propto t^{3/2}. \tag{2.11}$$

Because of the surface energy that exists of radius R, the temperature of equilibrium is shifted. If we assume the shift to follow the Gibbs-Thompson relation for a solid sphere, then we have

$$\Delta T \propto \frac{1}{t}. \tag{2.12}$$

Combining the three relation gives

$$\lambda \propto \Delta T^{-3/2}. \tag{2.13}$$

There are some assumptions made in this model that are far from obvious. The first is that the equation 2.12 is valid only for equilibrium, whereas our system is out of equilibrium. The second is that the twist is elastic.

Chapter 3

Experimental method

3.1 The sample

3.1.1 Chemical properties

In this study, I used an ethylene carbonate-polyacrylonitrile mixture. The chemical structures are shown in Fig. 3.1 . The chemical properties of ethylene carbonate are shown below.

Molecular weight	88.06
Melting point T_0	38.5^oC
Boiling point	248^oC
Density ρ (liquid, $T = 39^oC$	1.3218
$C_{p,liquid}(T = 323.15K)$	$133.9J.mol^{-1}.K^{-1}$
$C_{p,solid}(T = 298.15K)$	$117.44J.mol^{-1}.K^{-1}$
Latent Heat	$2.41kJ.mol^{-1}$
Caracteristic undercooling $\frac{L}{C_{p,l}}$	18.0^oC

The ethylene carbonate as purchased, was not very pure (concentration of impurities $\approx 2\%$). I

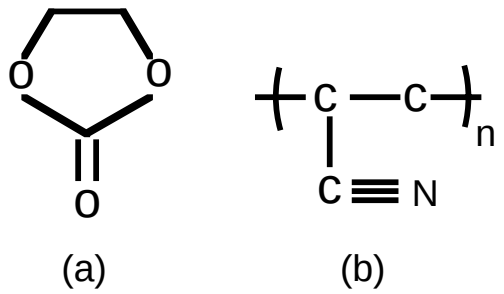

Figure 3.1: (a) ethylene carbonate; (b)Polyacrylonitrile.

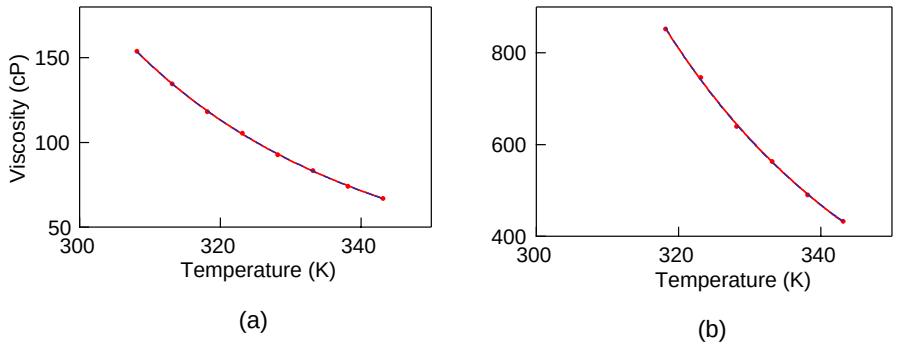

Figure 3.2: (a) Viscosity of a 5.8% mixture; (b) Viscosity of a 6.2% mixture. (Data collected by M. Degen)

purified it by recrystallization in ether. Basically, one saturates the warm solvent (ether) with EC and cools down the solution to recrystallize the EC. In the saturated solution, the impurities that were in the crystal are solubilized by the ether. After recrystallization, most of the impurities remain in the ether. The purified crystal can then be collected by filtering. I tried to estimate purity of the crystal after recrystallization by comparing the temperature difference between the liquidus and the solidus.[1] The difference is reduced by a factor of two after recrystallization, which means that the amount of impurities is around 1%. This method does not seem to be very efficient. I wasted a lot of ether to purify a small amount of EC, but I did not find any other solvant that would fit with the condition required for the recrystallization[2]. Therefore I kept on using this procedure. The amount of impurities should not change the properties of the banded spherulitic growth, as has been seen in the maleic anhydride-polyacrylonitrile mixture [1].

The viscosities of the 5.8% and 6.2% are shown in Fig. 3.2. We can see that the viscosity change drastically with the amount of polymer[3].

3.1.2 The system

Before I arrived in this lab, M. Degen and M. Case had already done some experiments on EC-PA mixtures. I tried to use their procedure, but it was cumbersome and results were hard to reproduce. Thus, I decided to build my own experiment. The required conditions were to make a sample with

[1] The liquidus temperature is the minimum temperature at which we cannot see any crystal whereas the solidus temperature is the maximum temperature at which we cannot see any liquid. In a pure crystal, those temperature are the same. In a mixture, the temperature differ, with the difference proportional to the impurity concentration in the dilute limit.

[2] At low temperatures, the EC must not be soluble in the solvant (or have very low solubility) but it must be soluble at high temperature.

[3] My results (below Fig. 4.8) suggests that the 5.8% mixture probably had a different polymer concentration (It would be around 3%)

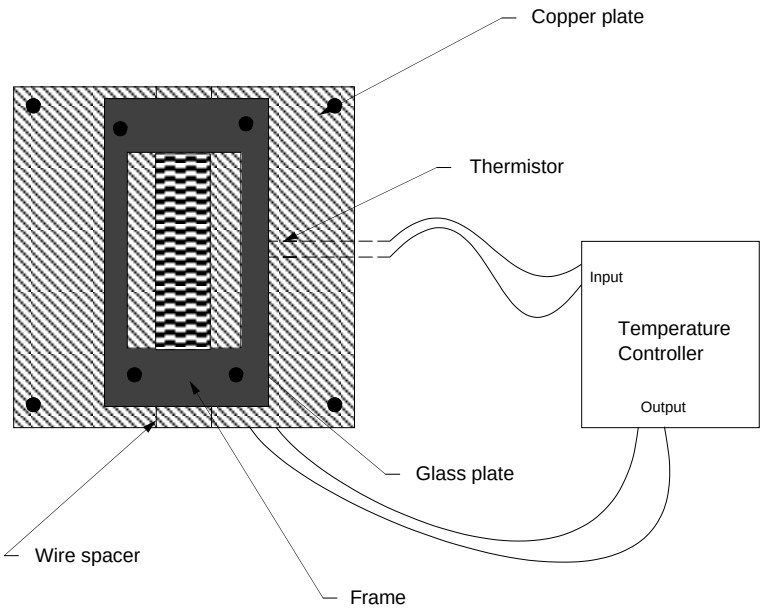

Figure 3.3: Top view

a well-defined thickness and to be able to control the temperature precisely. I made a cell with a bottom copper plate and a plate of glass with two wire spacers between. All of this was screwed together with a frame of aluminum. A copper plate was used in order to conduct away the latent heat released at the interface, which would otherwise increase the temperature of the front (see appendix). I controlled the temperature with a commercial regulator[4] that used a Peltier element[5] to heat or cool, depending on the polarity of the current passing through the device. The temperature was measured by a thermistor[6] glued inside the copper plate. Between the copper plate and the Peltier element, I added some glycerine in order to improve the thermal contact between those two. (Fig. 3.3 and Fig. 3.4).

I usually filled the cell by capillary action. I put a drop of the EC mixture on one edge of the glass plate and waited until the cell was full. Another method used was to put a drop between the glass and the copper and filling by squeezing with the screws. The second method was faster but was more likely to put some bubbles in the sample.

To initiate the crystallization, I usually put a small crystal on the edge of the plate with a needle after the temperature had stabilized.

[4] Wavelength Electronic HTC3000.
[5] Tellurex Co, CZ1-1.0-127-1.27 Z-max module.
[6] Thermometrics, P60.

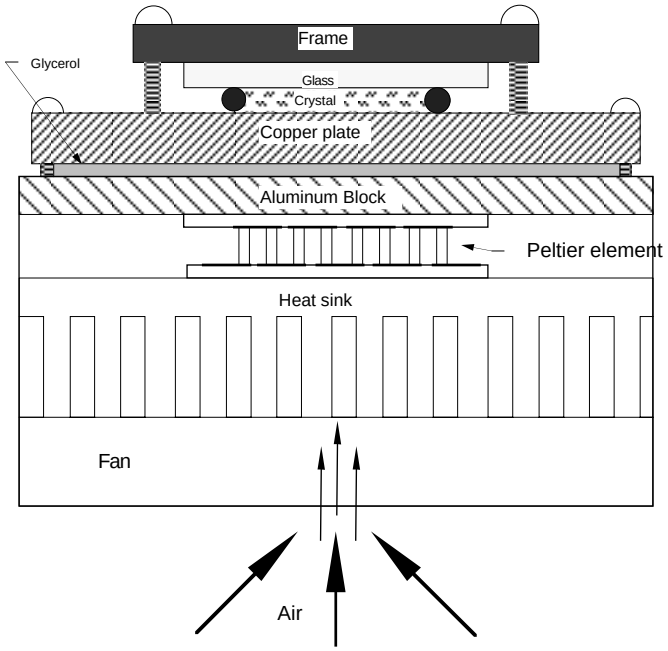

Figure 3.4: Side view

3.2 Calibration

3.2.1 Thermistor

Because every thermistor is different (readings vary about 5%), I had to calibrate each one. For that purpose, I immersed the copper plate in a water bath with a mercury thermometer. The data were fit to a standard phenomenological form for thermistors [11]: $T(R) = a + b\ln\left(\frac{R}{R_0}\right) + c\ln\left(\frac{R}{R_0}\right)^3$. I made two different copper plates, whose thermistors had the following coefficients:

	Plate 1	Plate 2
R_0	$11030.3k\Omega$	$10949k\Omega$
a	-79.3^oC	-80.1^oC
b	-10.9^oC	-10.9^oC
c	-0.1^oC	-0.1^oC

The typicaly systematic errors were $\pm 0.2^oC$. (see Fig. 3.5 Relative variations could be resolved to $10^{-4^o}C$ using precision multimeter[7] to measure the resistance.

[7] Keithley 2001 (7.5 digit precision)

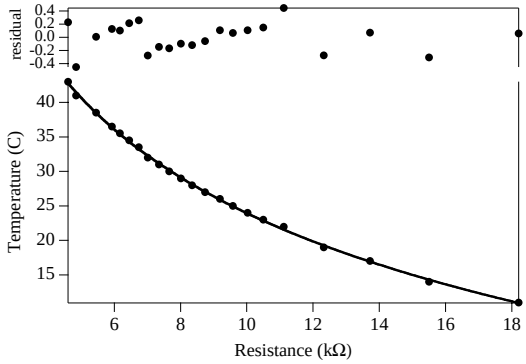

Figure 3.5: Calibration of the thermistor (plate 1)

3.2.2 Temperature-controller transfer function

In order to investigate the system response of the temperature controller, I tried to plot its transfer function defined as the rapport of the input over the output signal of the system as a function of the frequency of the input. I imposed a sinusoidal current in the Peltier and plotted the response of the thermistor inside the copper plate. The input signal used had the form $I = I_0(\cos(\omega t + \phi) + 0.5)$. The offset was present because I could not generate a bipolar signal. A more detailed study of the setup of the temperature controller can be found in the Appendix. In case of a semi-infinite material, the transfer function is

$$T(x,t) = \frac{1}{\sqrt{2}\lambda k} J_0 e^{-kx} e^{i\left(kx-\omega t+\frac{\pi}{4}\right)} + T_\infty, \tag{3.1}$$

here $k = \sqrt{\frac{\omega}{2D}}$, and $\lambda = D\rho c_p$.

In the appendix, we show that this approximate transfert function is ressonably accurate representation of the observed controller behavior.

3.3 Data acquisition

To acquire the data, we used a camera connected to a computer. The "NIH Image" program was used to process images.

Band spacing was measured simply by hand, making an average several bands.

Measuring the front velocity was more complicated as it is difficult to determine precisely the position of the front (and the precision must be better than the bands spacing). Therefore, I usually plot the average of the intensity along the direction of the growth. The position of the front was defined using a fixed valued of the intensity, as shown in Fig 3.6 (a). One difficulty with this method is that the light is not uniform throughout the sample. Thus, the threshold would depend on the position of the front. This can be seen in Fig. 3.6 where the intensity of the solid increase slightly. Another difficulty came from scratches on the copper plate that were visible in the profile.

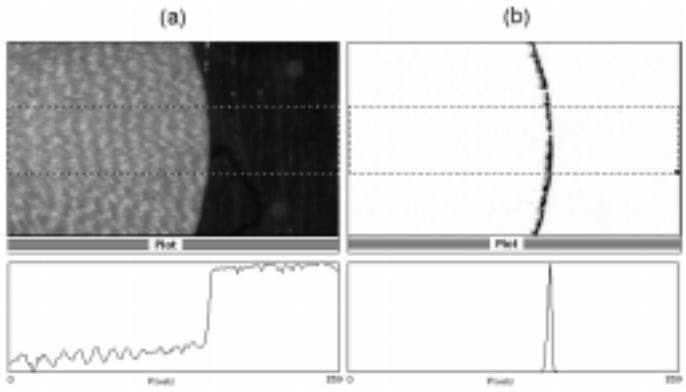

Figure 3.6: The two methods I have used to determine the position of the front: (a) shows the intensity plot, the front corresponds to a step of intensity; (b) shows the intensity plot after subtracting the same image from the preceding one. The front corresponds now to an intensity peak.

These problems were resolved by subtracting one image from the preceding one for every picture of the movie in order to remove static or slowly varying background features. The intensity profile that results is plotted and its peak corresponds to the position of the front between the two shots.

Distances are calibrated by taking a picture of a ruler.

Chapter 4

Experimental results

I continued my investigation of banded spherulites by looking at the features observed in other materials. I tried also to look at the dependence on the amount of polymer. But I did not have enough time to measure the viscosity of the different mixtures.

4.1 Band spacing

The most common feature of banded spherulites is that the band spacing depends on the undercooling. The first step was to investigate the dependence of band spacing when the undercooling is varying. One of the curves is shown in Fig. 4.1. Bands smaller than $0.1mm$ could not be studied for two reasons. The first is that the liquid freezes spontaneously for undercooling below $15^oC - 25^oC$. The other reason was that some scratches were present on the copper plate[1]. When band spacing were as small as those scratches, we could not distinguish the two. Band spacing greater than $3.5mm$ were seen.

We can see that the curve fits a power law. Nevertheless, the curve-fit parameters are quite different from what we expected. We can see that the curve diverges for a critical value of undercooling different from zero (In Fig. 4.1, this critical value is about $\Delta T^* = 4.89^oC$). Another different feature is that band spacing does not tend to zero as the undercooling tends to infinity.

One can notice that between Mike Degen's curve (Fig. 4.2) and my own (Fig. 4.1) the curve has been shifted horizontally. This shift resluts from the fact that the mixture was in contact with a plate of copper instead of only glass. It proved that the temperature was increased by about 5^oC in the previous set up because the latent heat generated by the moving front was not efficiently conducted away.

[1] We took great care in polishing the plates; however, we were unable to eliminate scratches and pits in the $100\mu m$ range.

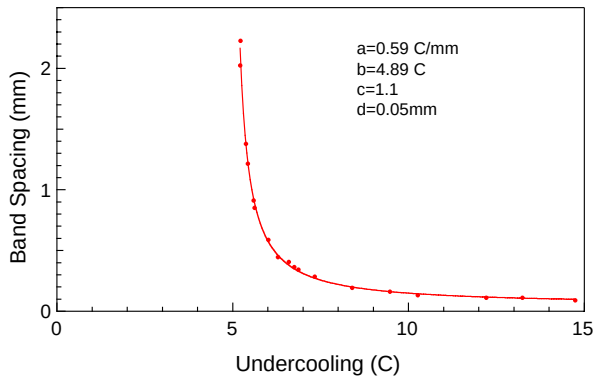

Figure 4.1: Band spacing versus undercooling, here the curve is fit with $BS(\Delta T) = a(\Delta T - b)^{-c} + d$. The concentration is 6.2% of Pa in ethylene carbonate.

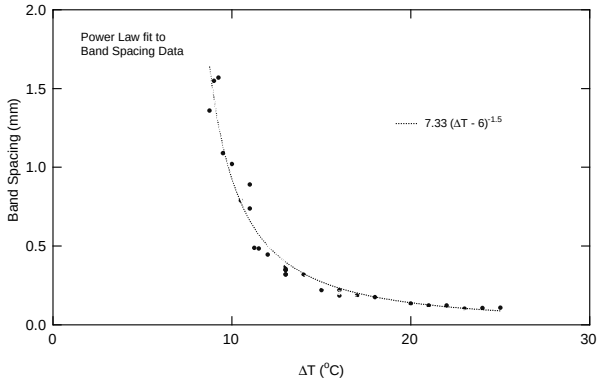

Figure 4.2: Band spacing versus undercooling for a 6.2% of PA in EC mixture using two glass plates.

As the band spacing depends of the undercooling (especially for small undercooling), it appears by looking at the variation of the bands in space that there was a temperature gradient throughout the plate. This gradient was less than $0.1^oC.cm^{-1}$. This gradient could explain why bigger bands spacing could not been seen. As the band spacing is more sensible of any fluctuation of the temperature near the critical undercooling, I would have need a smaller gradient to see large bands spacing. For example to see bands $4mm$ large, it would have required smallest variation of temperature than 0.01^oC over a distance of $4mm$. Gradient smaller than $0.02^0C.cm^{-1}$ would then have been required in order to see bigger bands.

The origin of this gradient remains unknown because the temperature seems to be higher on the edge of the plate than in the middle (If the gradient were due to any contact with the air, it would have been the other way wrong, because the temperature of the room was lower than the temperature of the sample). After the results presented here were obtained, we discovered that equilibriting the setup longer reduced the gradient by at least 50%. Thus most part of the gradient results from the top plate that was not in thermal equilibrium with the bottom plate.

As we fit the bands spacing with the curve $BS(\Delta T) = a(\Delta T - \Delta T^*)^{-c} + BS_\infty$, the uncertainty on the coefficients of the curve fitting were very high. This kind of curve depends extremely on the bigger band-spacings, that are the most uncertain as I explained upper. For example, if we ignore in Fig. 4.1 the two points that correspond of the biggest band-spacings, the coefficients become :

a	$0.55^oC.mm^{-1}$
b	5.05^oC
c	-0.82
d	$0mm$

The uncertainty on ΔT^* was very high because of the temperature gradient. If the measure were not taken in the same place, the band spacing can be different even if the temperature read is the same. That is why the curves could be shifted from an experiment to another even if the external parameter are then same because the camera does not look at the same place. In the experiment, the amplitude of the shift was about 0.2^oC. We will see below how I tried to sidestep this uncertainty by using another variable than the undercooling: the velocity of the front.

4.2 Front velocity

As the velocity of solidification depends on $\Delta\mu = \mu^s(T) - \mu^l(T)$ which depends on the undercooling, the velocity must depend on the undercooling. I tried to investigate this dependency. Therefore, I plotted the front position versus the time as shown in Fig. 4.7. One can verify that the velocity is more or less constant during one run. Looking at the residual, one can see that the velocity drift a little (the variations were about 5%), in particular that it is slower at the beginning and at the end of the sample.

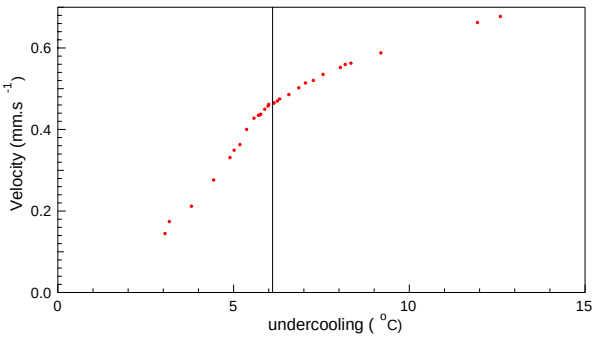

Figure 4.3: Velocity versus undercooling in a 6.4% mixture in PA. The vertical line denotes the starts of the bands.

Then I plotted the velocity vs. undercooling as shown in Fig. 4.3. As expected, the velocity increased with undercooling. Bands were seen from $\Delta T = 12.6^o C$ to $\Delta T = 5.7^o$. We can notice a change of the slope corresponding to a change of regime. Such correlations between the change of the slope and the change of the regime was studied by Hutter. [10] I did not study more precisely the regime transition, but it would be interesting to try to characterize any other regimes and their transitions.

Since the velocity increases monotonically with the undercooling, I could use the velocity rather the undercooling as an external parameter. This also eliminates any uncertainty about the temperature due to the gradient, latent heat or any other effects that might induce a systematic difference between the temperature of the front and the temperature read by the thermistor. This result can be correlated to Hutter's observations [9] who compared the band spacing versus velocity by using a free growth solidification and a directional solidification[2] in a liquid crystal. He showed that the curve is the same for the two kinds of experiments. That suggests that only one of the two parameter determines the band spacing.

Bands spacing vs. velocity is shown in Fig. 4.4. We can expect that the curve fits with $v = a(\Delta T - b)^c + d$.

As I discussed above, by plotting the band spacing vs. velocity eliminates the effect of the latent heat. We know that the latent heat released depends on the thickness of the sample since the it depends on the volume of the liquid freezed. With this method, I can determine any effect of the thickness of the sample beside the increase of the temperature of the front due to the latent heat.

[2] The directional solidification consists in moving the sample with a constant velocity in a fixed temperature gradient. This method allows to fix the solidification-front velocity rather than the undercooling temperature.

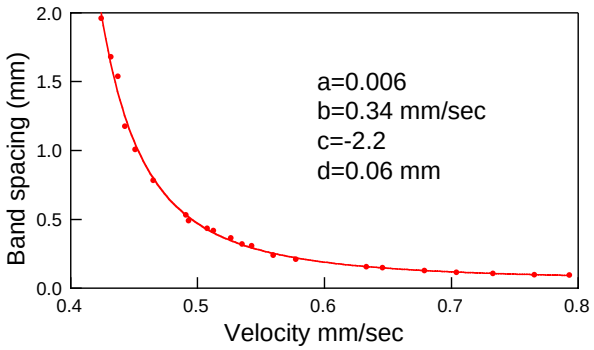

Figure 4.4: Band spacing versus velocity in a 6.4% mixture in PA. The curve is fit with $BS = a(v-b)^c + d$.

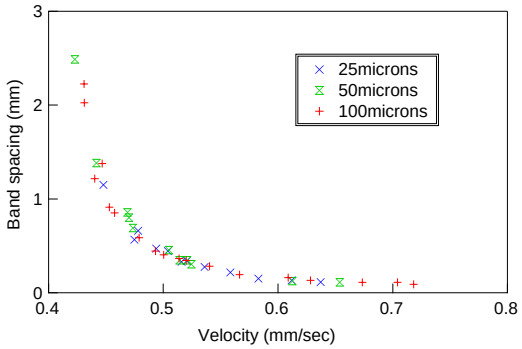

Figure 4.5: Band spacing versus velocity, using different thickness in a 6.2% mixture of PA in EC.

4.3 Thickness

In order to investigate the influence of the thickness of the sample, I studied the the band spacing of different sample with different thickness. I used the following different thickness : $25\mu m$, $50\mu m$, $100\mu m$ with a 6.2% mixture of PA in EC. The curves of the band spacing versus velocity is shown in Fig. 4.5.

One can see that all the data seem to fit to the same curve[3]. This suggests that sample thickness has no fundamental effect on band spacing.

4.4 Core region

The next step of my study was to investigate the dependence of the core region on the undercooling. In this kind of mixture, I could see a core region as shown in Fig. 4.6. The previous experiment on maleic anhydride predicts that the core region diverges at a critical undercooling higher than

[3]It is so for the Mike Degen's curve which $198mm$-thick sample.

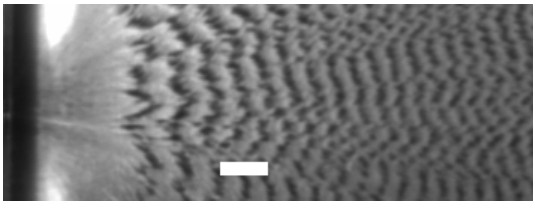

Figure 4.6: Core of a 6.2% of PA in Ec mixture. the temperature is $28.96^{o}C$. The scale bar is 1 mm.

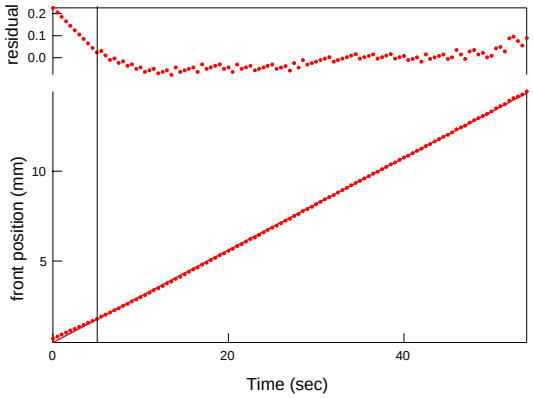

Figure 4.7: Position of the front versus the time, the mixture is 6.2% of PA in EC. The vertical line corresponds to the first band appearance. The slope is different at the beginning ($0.22mm.sec^{-1}$) than in the middle($0.25mm.sec^{-1}$) that is due to a change of the temperature.

the band-spacing–divergence one. [1] Another study claims that we should see a change in the velocity when the first band appears [10], since it corresponds to a regime transition. The cores I saw seemed to depend strongly on the temperature: the core size increased as the undercooling decreased. Unfortunately when I tried to investigate the front velocity, I realized that the core region might be correlated with the temperature gradient of my system. As shown in Fig. 4.7, the velocity is slower (because the temperature is higher) at the beginning than in the middle of the sample. We also verified temperature change by looking at the band-spacing variation (Fig. 4.6). Thus I could not determine whether the bands appear because of the size of the core or because the temperature decreases, without modifying my system.

To study more precisely the core region, I would have had to start the crystallization in the middle in the sample. I tried to drill a small hole in the glass plate. Unfortunately, I could not manage to drill a hole whose diameter was smaller than $1mm$, and that was not small enough to eliminate the temperature gradient. I thus decided to stop investigating the core region in order to study the dependence of band spacing on mixture viscosity of the mixture, which did not require me to change my system.

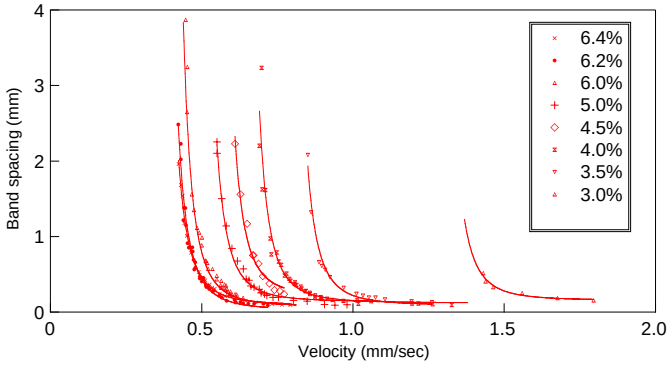

Figure 4.8: Different curve of Band spacing-velocity when the concentration is varying.

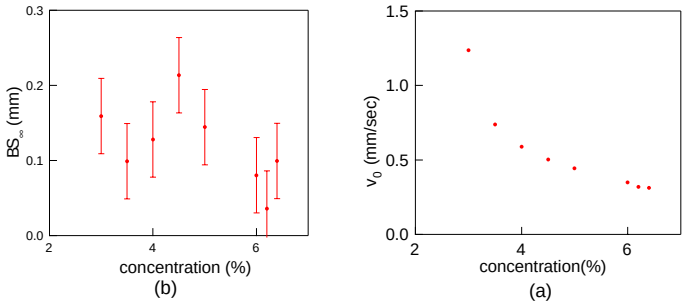

Figure 4.9: Dependency of the coefficient v_0 and BS_∞ on the concentration

4.5 Dependence of the viscosity

In order to investigate the dependency of the fluid viscosity, I prepared different mixtures with different polymer concentrations as the viscosity increases with concentration. Unfortunately, I did not have time to measure the viscosity of each mixture. I made the following different concentrations: 3.0%, 3.5%, 4.0%, 4.5%, 5.0%, 6.0%, 6.2% and 6.4%. I did not prepare lower concentrations because the bands became less and less visible as the viscosity decreased. In particular, the band spacing loses a "coherence" throughout the sample, the global pattern was becoming granular. In the 3.0% mixture, I did not manage to have more than ten points. The curves are shown in Fig. 4.8. We can see that the properties of the bands are sensitive to the viscosity.

One can notice that the curves seem to be similar. Thus I tried to fit globally all the curves with $BS = a(v - v_0)^b + BS_\infty$ using a common value of a and b. The curve global fit is plotted in Fig. 4.8. The coefficients obtained :

a	0.0015
b	-3.2

Since v_0 and BS_∞ depend on the concentration, I tried to figure out if there was a trend or not. Therefore I plotted the curves $v_0(concentration)$ and $BS_\infty(concentration)$ as shown in Fig. 4.9.

We note that the divergence point of the velocity(v_0) depends sensitively on the concentration. The dependence on the concentration seems to be greater for small concentrations. I would have needed more data for small concentrations to confirm this because the uncertainty there is higher than at larger concentration. As I said above, this uncertainty is due to the fact that bands are harder to see for small concentration.

The trend for BS_∞ is more difficult to see. I plotted the error bars in Fig. 4.9 given by the procedure when I fitted the curve BS-velocity. They are very large compared to the values of BS_∞. My system was not precise enough to be able to see the small bands at high undercoolings. It would have been usefull to modify the system in order to be able to look with a microscope. It would then be easier to make the difference between the scratches and the bands by using a polarizer and an analyzer, since the bands result from a crystal-axis rotation.

The high sensitivity to the viscosity variations might suggest that banding is due to an hydronynamical flow effect but no theory has been proposed to describe this.

Chapter 5

Conclusion

I have shown that the banded spherulites seen in ethylene-carbonate–Polyacrylonitrile mixture have properties similar to those seen in other materials. In particular, the band spacing vs. undercooling and band spacing vs. front velocity curves fits a power-law curve, as expected. There are, however some essential differences. The band spacing vs. undercooling fit is a curve $BS = a(\Delta T - \Delta T^*)^b + BS_\infty$, with ΔT^* and BS_∞ different from zero. No explanation has been proposed for this fact. I also showed that the thickness of the sample has no effect on the band spacing besides increasing the temperature of the front. I studied the concentration dependence of the mixture. I showed that it affects greatly the band spacing-vs-velocity curve. This suggests that the viscosity of the liquid might be an important parameter influencing the band spacing, which could give some clue for finding out the banded-spherulite mechanism.

Future investigation should examine more precisely the core region, in order to see whether it is responsible for the fact that we do not see greater band spacing. It is also necessary to continue the study of the viscosity. To acquire more data with small concentration would give a better idea of its effect. This would maybe require a microscope rather than a camera. One has to measure the viscosity of the different mixture to know determine quantitatively its influence. Those investigations could lead to a better understanding of the phenomena.

But there are many investigation possible to understand better banding. We can try to look with an electron microscope or with an atomic-force microscope the structure of the crystallites.

Appendix: The temperature controller

Because the probe and the heater are not exactly at the same place, there is a time lag between the output and the input of the temperature controller. This can lead to oscillation of the temperature. In order to study the stability of the system, we calculate the response of the probe when we apply an oscillating signal in the Peltier.

Consider a semi-infinite material extending from $x = 0$ to $x = +\infty$. We apply an oscillating heat current at $x = 0$: $J_Q(x = 0) = J_0 e^{-i\omega t}$ The temperature field satisfies the diffusion equation in the material:

$$D\Delta T - \frac{\partial T}{\partial t} = 0. \tag{5.1}$$

Here, D represents the thermal diffusion constant of the material. If we assume that the solution is of the form

$$T(x,t) = f(x)e^{-i\omega t} + T_\infty\,,$$

then $f(x)$ obeys

$$D\ddot{f}(x) + i\omega f(x) = 0. \tag{5.2}$$

The solution to this equation is

$$f(x) = Ae^{(k-ik)x} + Be^{(-k+ik)x,} \tag{5.3}$$

where $k = \sqrt{\frac{\omega}{2D}}$. The two boundary conditions are

$$\begin{cases} T(x \to +\infty) = T_\infty\,, \\ -D\rho c_p \frac{\partial T(0,t)}{\partial x} = J_Q(x=0) \quad \text{that is the Fourier equation applied at } x = 0, \end{cases} \tag{5.4}$$

where ρ represents the density of the material and c_p is the heat capacity per unit mass (at constant pressure). The solution of Eq. 5.1 is

$$T(x,t) = \frac{1}{\sqrt{2}\lambda k} J_0 e^{-kx} e^{i\left(kx-\omega t+\frac{\pi}{4}\right)} + T_\infty \tag{5.5}$$

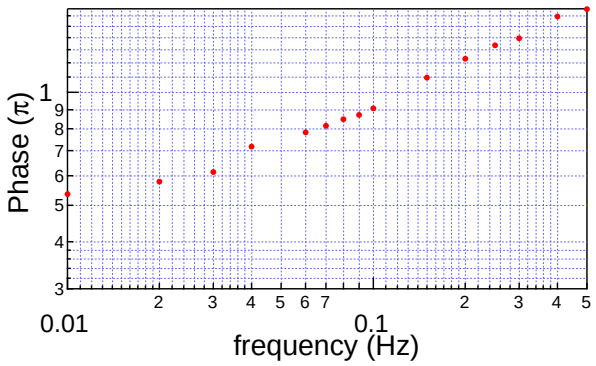

Figure 5.1: Phase response of the transfer function

Since the temperature controller is a proportional controller, we have

$$J_0 = G[T(\ell) - T_\infty], \tag{5.6}$$

where G is the gain of the controller and ℓ is the distance between the temperature probe and the Peltier element. From Eqs. 5.1–5.6, an also from a linear stability analysis we can find ω^* and G^* corresponding to the limits of the stability. They are given by [12]

$$\begin{cases} k^*\ell + \frac{\pi}{4} = \pi, \\ G^* \frac{1}{\sqrt{2}\lambda k^*} e^{-k^*\ell} = 1. \end{cases} \tag{5.7}$$

Thus

$$\begin{cases} \omega^* = 2D\left(\frac{3\pi}{4\ell}\right)^2 \propto \frac{D}{\ell^2}, \\ G^* = \frac{3\pi\lambda\sqrt{2}e^{-\frac{\pi}{4}}}{4\ell} \propto \frac{\lambda}{\ell}. \end{cases} \tag{5.8}$$

From this equation we can see that in order to have a high gain (what would reduce the time constant of the temperature controller) we need to have a small distance ℓ between the probe and the heat source. Since this distance is fixed by the system, I can improve the temperature control by increasing λ. This explain why I used a copper plate, which has a high heat conductivity and why I put some glycerol between the plate and the Peltier element.

The phase of the transfer function is shown in Fig. 5.1. One can see that there is a kink in that curve and that it for small frequency is different from the expected one in the appendix. This is due to the fact that for low frequency (large characteristic length $(1/k)$, one cannot approximate the material as semi-infinite. One can also see one that curve that the frequency is about 0.1 Hz This is a little high, and in my opinion, is due to the thermal conductivity of the glue used to fix the thermistor to the copper plate.

The temperature controller built with appropriate gain, could reach a steady state[1] in 2 mn.

[1] I considered that the steady state was reached when the amplitude of the oscillation was smaller than 0.005^oC

Appendix: temperature rise at the interface

The calcul of the temperature increase was made by Hutter [9] when the liquid is bounded by two semi-infinite plate of of glass. The temperature found was

$$\delta T = -\frac{Lvd}{2\pi D\rho c} K_0(\frac{vd}{4\pi D}), \tag{5.9}$$

where v is the front velocity and d is the sample thickness. Using the dimensionless variable $x = \frac{vd}{D}$, we have

$$\begin{cases} \delta T = \frac{L}{\rho c} h(X) & \text{with} \\ h(X) = -\frac{X}{2\pi} K_0(\frac{X}{4\pi}). \end{cases} \tag{5.10}$$

Since my system is bounded with a plate of copper, this calculation overestimate the real temperature increase. To bound the real temperature increase I propose to calculate with a sample bounded by two perfect thermal conductor, which has a constant temperature. I starts with the assumption of a planar interface of thickness d in the y-direction propagating at a constant velocity v in the x-direction (see Fig. 5.2). We take the lengh tof the front in the z-direction as infinite. The

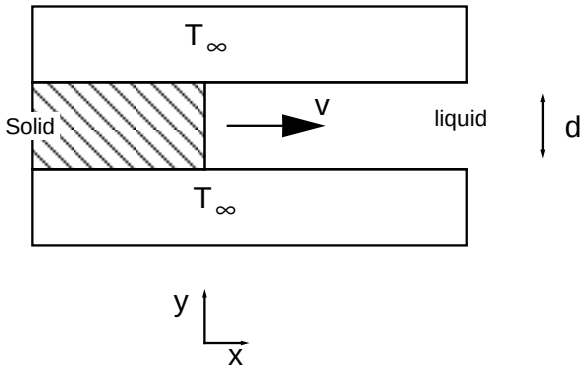

Figure 5.2: Front de solidification bounds by two plate of perfect heat-conductor

temperature field $T(x, y, z)$ satisfy in the referency in which the front is static

$$\nabla^2 T + \frac{v}{D}\frac{\partial T}{\partial x} = 0. \tag{5.11}$$

The boundary conditions are

$$\begin{cases} T(|x| \to +\infty) = T_\infty \\ T\,|_{x=0} \;= T\,|_{x=d} \;= T_\infty \\ \frac{\partial T}{\partial x}\,|_{x=0+} \;- \frac{\partial T}{\partial x}\,|_{x=0-} \;= \frac{Lv}{D\rho c} \end{cases} \tag{5.12}$$

If we assume a solution to Eqs. 5.11–5.12 of the form

$$T = T_\infty + u(x, y)e^{-\frac{x}{\ell}}, \tag{5.13}$$

where $\ell = 2D/v$, we find that u must satisfy the equation

$$(\partial_{xx} + \partial_{yy} - \frac{2}{\ell})u = 0 \tag{5.14}$$

Assuming a solution to this equation is of the form

$$u(x\,, y) = \sum_{n=0}^{\infty} f_n(x) \sin n\frac{y\pi}{d}, \tag{5.15}$$

then $f_n(x)$ must satisfy

$$\frac{\ddot{f}_n(x)}{f_n(x)} - k_n^2 - \frac{2}{\ell} = 0, \tag{5.16}$$

where $k_n = n\frac{\pi}{d}$. Then we have

$$f_n = A_n e^{-x\sqrt{(\frac{2}{\ell})^2 + k_n^2}}. \tag{5.17}$$

The boundary condition (Eq. 5.12) determines A_n

$$2A_n\sqrt{\frac{2}{\ell} + k_n^2} = \frac{Lv}{D\rho c}. \tag{5.18}$$

Thus the solution is

$$u(x, y) = \sum_{n=0}^{\infty} \frac{Lv}{2D\rho c\sqrt{(\frac{2}{\ell})^2 + (n\frac{\pi}{d})^2}} \sin\,(n\frac{y\pi}{d})e^{-x\sqrt{(\frac{2}{\ell})^2 + (n\frac{\pi}{d})^2}}. \tag{5.19}$$

The temperature-increase peak is then

$$\begin{cases} \delta T = \frac{L}{\rho c} z(X) & \text{with} \\ z(X) = \sum_{n=1}^{\infty} \frac{(-1)^{n+1}}{\sqrt{2 + 4(2n-1)^2(\frac{\pi}{X})^2}} \end{cases} \tag{5.20}$$

I plotted the two function $z(x)$ and $z(x)$ in Fig. 5.3

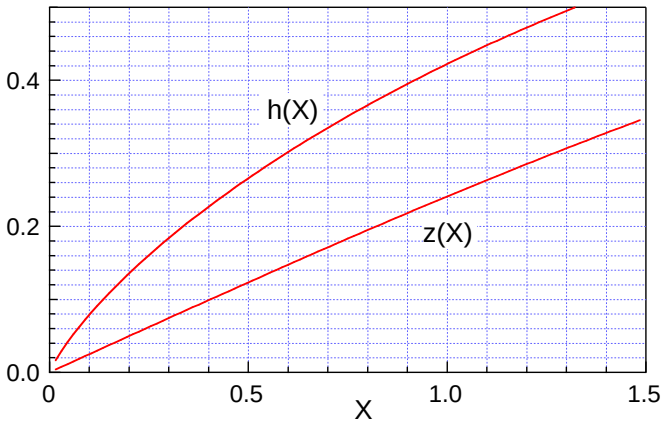

Figure 5.3: Plot of $h(X)$ and $z(X)$.

In our case, if we take $v = 0.4mm.s^{-1}$, $D = 10^{-3}cm^2.s^{-1}$, $d = 0.100mm$ and $\frac{L}{\rho c} = 18^oC$, then we have: $h(X) \approx 4^oC$ and $z(x) \approx 0.9^oC$. We can see now why it is necessary to conduct the heat away in order to reduce the temperature increase. The shift seen between M. Degen's band-spacing vs. undercooling and mine can be explain by the fact that his case was close to the approximation of semi-infinite glass plate and mine was closer to the ideal heat-conductor, as the copper is a better heat-conductor than glass.

Bibliography

[1] M.M Degen, N. Costanzino and J. Bechhoefer, "On the properties of Large banded spherulites in a Maleic Anhydride-Polyacrylonitrile Mixture," *J. Cryst. Growth* **209** (200)

[2] A.J. Owen, "A Note on Twist-Banding in Spherulites of Poly(3-hydroxybutryate)," *Polymer Communication* **38**, 3705-3708 (1997).

[3] H.D. Keith, F.J Padden, Jr., J. Appl. Phys. **34**, 2409-2421 (1963)

[4] W.A Tiller, *The Science Of Crystallization: Macroscopic Phenomena and Defect Generation.* 342-346 (Cambridge University Press, Cambridge, 1991).

[5] W.W Mullins and R.F Sekerka, "Stability of a Planar Interface During Solidification of a Dilute Binary Alloy," *J. Appl Phy.* **35**, 444-451 (1964).

[6] H.D. Keith, F.J Padden, Jr., "Twisting Orientation and the Role of Transient states in Polymer Crystal," *polymer paper* **25**, 28-42 (1983).

[7] J. Bisault, G. Ryschenkow and G. Faivre, "Spherulitic Branching in the Crystallization of Liquid Selenium," *J. Cryst. Growth* **110**, 889-909 (1991).

[8] L. Landau, E Lifchitz, *Théorie de l'élasticité*, 58-59. (Édition de Moscou, Moscou, 1967)

[9] J.H. Hutter, "Solidification of a Liquid Crystal: Morphologies and Transitions." 63-70 (Thesis, Simon Fraser University, 1997).

[10] Jeffrey L. Hutter, John Bechhoefer, "Many modes of rapid solidification in a liquid crystal," *Physica A* **239**, 103-110 (1997).

[11] J.H Moore, C.C. Davis, M.A Coplan, *Building Scientific Apparatus*, 515-516 (Addison Wesley, 1989).

[12] K. Dutton, S. Thompson, B. Barraclough, "The Art of Control Engineering", 214-215 (Addison Wesley, 1997).